



Spatio-temporal interpolation and delineation of extreme heat events in California between 2017 and 2021



Pedram Fard^a, Ming Kei (Jake) Chung^{a,c,d}, Hossein Estiri^b, Chirag J. Patel^{a,*}

^a Department of Biomedical Informatics, Harvard Medical School, Boston, MA, USA

^b Department of Medicine, Harvard Medical School, Boston, MA, USA

^c School of Public Health and Primary Care, The Chinese University of Hong Kong, Hong Kong SAR, China

^d Institute of Environment, Energy and Sustainability, The Chinese University of Hong Kong, Hong Kong, China

ARTICLE INFO

Handling Editor: Jose L Domingo

Keywords:

Heat-health impacts
Apparent temperature
Spatio-temporal modeling
Distance-based interpolation
Augmented mapping
Climate change

ABSTRACT

Robust spatio-temporal delineation of extreme climate events and accurate identification of areas that are impacted by an event is a prerequisite for identifying population-level and health-related risks. In prior research, attributes such as temperature and humidity have often been linearly assigned to the population of the study unit from the closest weather station. This could result in inaccurate event delineation and biased assessment of extreme heat exposure. We have developed a spatio-temporal model to dynamically delineate boundaries for Extreme Heat Events (EHE) across space and over time, using a relative measure of Apparent Temperature (AT). Our surface interpolation approach offers a higher spatio-temporal resolution compared to the standard nearest-station (NS) assignment method. We show that the proposed approach can provide at least 80.8 percent improvement in identification of areas and populations impacted by EHEs. This improvement in average adjusts the misclassification of about one million Californians per day of an extreme event, who would be either unidentified or misidentified under EHEs between 2017 and 2021.

1. Introduction

Extreme Heat Events (EHE), are increasingly recognized as associated with adverse health outcomes (Romanello et al., 2022; Sheridan et al., 2019; Ebi et al., 2021; Luber and McGeehin, 2008). It is hypothesized that EHE can lead to a broad range of morbidity from adverse maternal and birth outcomes (Ilango et al., 2020; Kuehn and McCormick, 2017) to exacerbated pre-existing conditions (BYXiang et al., 2019; Soneja et al., 2016), negative mental health impacts (Nori-Sarma et al., 2022; Thompson et al., 2018) and cardiovascular and respiratory hospitalization (Ebi et al., 2021; Cheng et al., 2019). EHE may also impact health services demand and impose a substantial economic burden on healthcare systems (BYXiang et al., 2019). Early studies suggested differences in effect of EHE on mortality and morbidity due to the timing, duration, and intensity of the events (Anderson and Bell, 2011; Ellis and Nelson, 1978; Schuman, 1972). Studies also reported the health risks associated with EHE are exacerbated by socioeconomic and demographic factors, where children, elderly, racial and ethnic groups and low-income individuals tend to be impacted disproportionately (BYXiang et al., 2019; Hoehne et al., 2018; Gronlund et al., 2015; Fisher

et al., 2017; Vanos et al., 2017).

To quantify the potential health risks and physiological impacts of EHEs, a very first step is to identify the geographic and temporal extent of the extreme heat episodes (Horton et al., 2016). A clearly delineated EHE boundary helps to better estimate the population at risk (Hass et al., 2021). Earlier studies have investigated the health risks in association with temperature on a per-degree basis at aggregate spatial scale, while less attention was given to delineating the extreme events geography (Fisher et al., 2017; Gasparrini et al., 2015). Over time, different stationary methods have been developed to spatially detect EHE using a temperature measure or composite heat indices (Sheridan et al., 2019; Nairn and Fawcett, 2014; Tuholkske et al., 2021; Vaneckova et al., 2010).

In identifying the geographic areas that are impacted by EHE, accurate spatiotemporal delineation has often been compromised in favor of simplicity (Tuholkske et al., 2021). Attribution of the impacts has been classically determined by applying static methodologies in which the population of the study unit (e.g., census tract, zip/postal code, city) is linearly assigned temperature data from the closest weather station (nearest neighbor/sensor) (Sheridan et al., 2019; Kwan, 2018; Delmelle et al., 2022). As frequency and intensity of EHE is on the rise globally

* Corresponding author. 10 Shattuck St., Boston, MA 02115, United States.

E-mail address: Chirag.Patel@hms.harvard.edu (C.J. Patel).

(Romanello et al., 2022), enhancing the EHE delineation methods can help us better understand the increasing risks of these events. The spatial interpolation method has shown to be a viable solution by estimating continuous spatial surfaces from sparse spatial samples or data points (Horton et al., 2016; Chun et al., 2019; Chowienczyk et al., 2020).

A major challenge in investigating the health impacts of EHE is the ambiguity of the “extreme event” definition (Horton et al., 2016; Sheridan and Lee, 2018). In earlier studies, an EHE was often identified as the sustained period of high temperature also known as “heatwave” (Cheng et al., 2019; Anderson and Bell, 2011; Zhang et al., 2017; Åström et al., 2011). The absolute temperature thresholds were used to mark the EHEs or heatwaves (Sheridan et al., 2019). For example, the Heat and Health Tracker, a national reference portal of US Centers for Disease Control and Prevention (CDC) that identifies the population at EHE risk uses daily maximum temperature above 90 °F (~32 °C) as indicator of extreme heat (National Environmental Public Health Tracking Network). On the other hand, a growing body of research has been developed upon the relative temperature measures through localized and day-specific thresholds (Nori-Sarma et al., 2022; Fisher et al., 2017; Hajat and Kosatky, 2010). In such an approach, the threshold is determined based on the historical temperature distributions over an extended period of time (i.e., 10–30 years). Relative thresholds take into account the temperature anomalies, which are deviations from the long-term average temperature (Fisher et al., 2017; Sheridan et al., 2020). Despite improving generalizability of the results, relative thresholds tend to obscure the intuition that simple absolute thresholds provide (Horton et al., 2016).

Much of the prior EHE research have leveraged a composite measure of heat exposure by factoring relative humidity and wind speed in addition to the ambient temperature, as these parameters impact thermoregulation processes (Hajat and Kosatky, 2010; Isaksen et al., 2016; Spangler et al., 2019) including sweating as an important measure of thermoregulation. The sweat evaporation rate depends on the temperature and relative humidity and airflow velocity in the environment (Sherwood and Huber, 2010). Along with different choices of temperature measure, the daily temporal resolution has been broadly used to define EHE. Some studies specified isolated hot days as independent events (Fisher et al., 2017), others have considered EHE as an extended period where the temperature exceeds a certain threshold for two or more consecutive days (Anderson and Bell, 2011; National Environmental Public Health Tracking Network; Cheng et al., 2018). Different definitions of EHEs can lead to different conclusions about the frequency and severity of such events. The inconsistencies of EHE’s health impacts reported in prior research have been frequently attributed to the heterogeneous methodologies and criteria used in EHE identification (Fisher et al., 2017; Hajat and Kosatky, 2010).

We have developed a spatio-temporal methodology to dynamically delineate EHE across space and time at a fine spatial resolution (600m) and daily intervals. We introduced a new indicator of excess heat to quantify the EHE severity, and to delineate geography of EHEs. Using publicly accessible climate data from NOAA (National Climatic Data Center and U.S. Department of Commerce, 2001) we computed a composite measure of heat exposure and examined our spatial interpolation method in a case study in California, during a 5-year period between 2017 and 2021. Our results suggest significant improvement (15.8%–30.5%) in apparent temperature (AT) estimates, and in identifying the population who would be misclassified by the standard nearest-weather station approach (at least 62.7% of the impacted Californians in 60% of the EHE days), compared to our proposed method.

2. Methods

We have developed a geo-informatics pipeline (Fig. 1) that, (1) delineates the spatio-temporal boundaries for the EHE using the excess heat factor (EHF) metric (Nairn and Fawcett, 2014) and the statistically defined extreme heat thresholds (Sheridan et al., 2019), (2) identifies

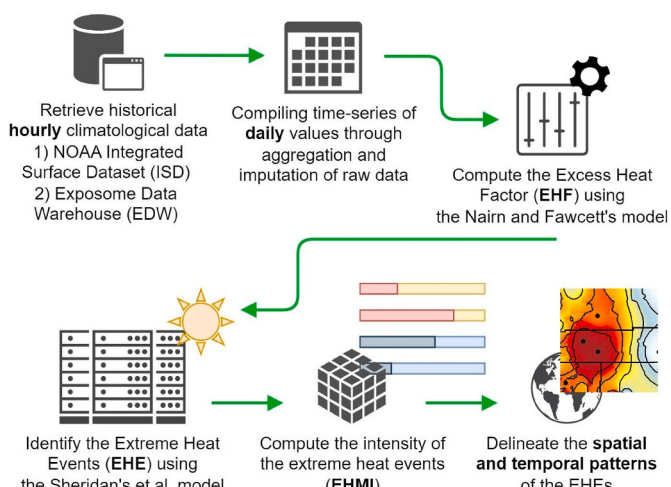


Fig. 1. Schematic diagram of the implemented method and data pipeline for extreme events detection.

area and population impacted by EHE in a daily interval.

We validated our spatial interpolation method in estimating temperature for multiple sets of sampled stations. We also compared the area and population impacted by the EHE between the dynamic spatiotemporal interpolated surfaces and the nearest-station (NS) approaches.

2.1. Data records and pre-processing

We measured the AT that quantifies how hot the weather “feels” when relative humidity and wind speed factored in with the actual ambient temperature. AT as formulated by Steadman (1984), is computed through linear combination of actual temperature, vapor pressure and wind speed in the metric units. AT is interpreted in Celsius (°C), where:

$$AT = -2.7 + 1.04T + 2.0P - 0.65u \quad (1)$$

AT: Apparent Temperature Index in °C.

T: Temperature in °C.

P: Vapor pressure in kPa

u: Wind speed in m/s.

To calculate AT, we used historical climatological data at station level obtained from the Integrated Surface Database (ISD) (National Climatic Data Center and U.S. Department of Commerce, 2001). The ISD is a publicly accessible data source provided by the National Oceanic and Atmospheric Administration (NOAA) with global coverage. We retrieved the climatological records for a 5-year period between 2017 and 2021. In addition, for computation of the acclimatization term during onset of the study period (January 2017), we included values from the prior 30 days, back to December 2016. We identified a set of 202 stations including 167 locations within the State of California, and 35 additional stations within a 100 km (~62 miles) buffer, inside neighboring states of Nevada, Arizona, Oregon. The additional stations were instrumental in improving the estimates along the border areas of California, where lower concentration of weather stations could deviate the spatial interpolation estimates.

The combined yearly tables contained more than 16.5 million records of hourly and sub-hourly weather parameters including temperature (TMP), dew point temperature (DEW) and wind speed (WND). We used “humidity” library (Cai, 2019) in R to compute the vapor pressure from the dew point temperature values. Although ISD provides a rich set of climatological variables and temporal coverage, the collected raw data had patterns of missingness. Fig. 2 presents an example of a missingness pattern identified for a certain station. It illustrates the data for a

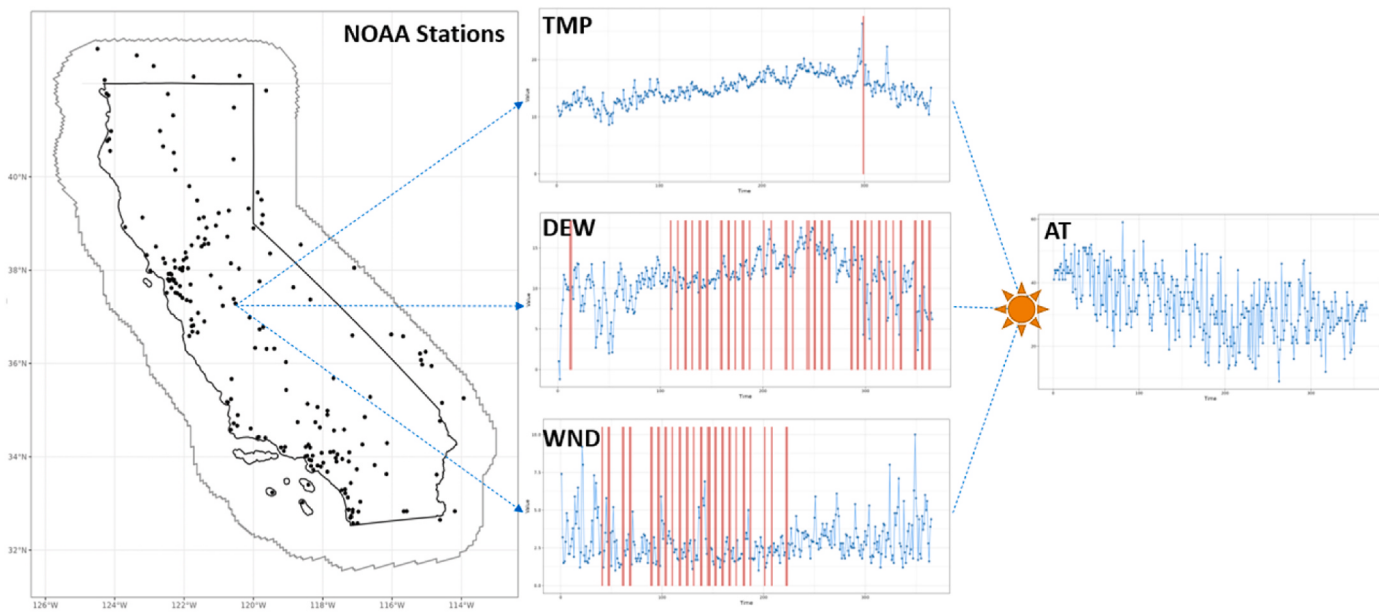


Fig. 2. An example of missingness patterns for a certain station, along with the derived AT computed based on the imputed missing values. Red lines denote missing data; blue points denote non-missing daily data points.

particular station, covering a time span of one year. The available (non-missing) data points for each day are represented using blue dots. In contrast, each red line indicates missing value of a daily climatological variable for the same station. To assess the extent of missingness within the entire data set we introduced a simple measure called "Completeness Indicator". This measure reflects the ratio of the number of days per year that all the three variables of interest (i.e., TMP, DEW, WND) were present for a given station.

We identified a broad range of completeness levels, and various patterns of missingness across different station locations and over time (Fig. 3). For example, looking at the 75% Completeness Index level (yellow line), we observe that more than 40 out of 202 stations had at least 25% (or 90) days missing data every year between 2017 and 2021.

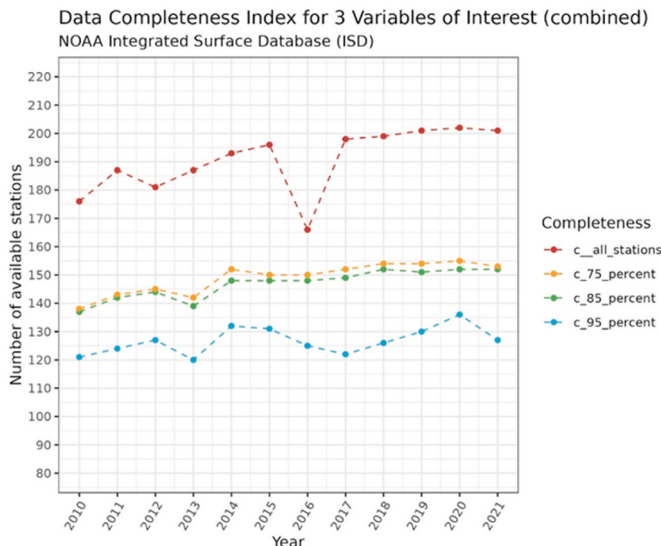


Fig. 3. Total number of available NOAA stations within the study area along with the number of stations satisfying different levels of Completeness Index (2010–2021). The Completeness levels in this figure are denoted as follows: c_all_stations: no completeness criteria applied (in red); c_75_percent: 75 percent completeness (in yellow); c_85_percent: 85 percent completeness (in green); c_95_percent: 95 percent completeness (in blue).

We applied a two-step pre-processing approach to resolve missingness through temporal aggregation and imputation. First, we aggregated the hourly and sub-hourly readings into average daily values for temperature, dew point temperature and wind speed. Second, we only included stations ($n = 135$) that contained daily values for all the three variables, at least in 95% of the days per year (347 days) (Fig. 3, blue line).

We then imputed missing values in the curated data set using two imputation methods. In order to fill the missing gaps with up to three consecutive days, we applied a linear interpolation algorithm to populate the values by considering the day before and the day after the gaps (Moritz and Bartz-Beielstein, 2017). Using the interpolation method we imputed 1281 TMP, 1367 DEW, and 1095 WND values. In addition, the Kalman smoothing method was used for imputing larger than three-day gaps in the time-series of daily values (Afrifa-Yamoah et al., 2020). The Kalman algorithm incorporates not only the near observations but also information from past patterns that allows us to take advantage of the temporal structure in the data. It optimally combines the prior state estimate with the current observation minimizing uncertainties associated with estimates (Peckham, 2017). We imputed 218 TMP, 228 DEW, and 174 WND values using Kalman smoothing method.

2.2. Validation of temperature estimates

To validate our spatial interpolation method, we trained two models using the standard nearest-station and our interpolation methods with 80-20 training-to-testing ratio. The training set stations are shown as solid circles, and the held-out test set stations are presented as blank rectangles in Fig. 4. The color gradient in this figure ranges from blue to red, indicating the values of the AT for the underlying areas. The regions in shades of blue represent colder temperatures, while the areas in red represent warmer temperatures. We performed five iterations of random train-test sampling with replacement to be able to provide more robust estimates of the error with confidence intervals. At each iteration, the test set ($n = 27$) stations were randomly selected from those stations that were located in California. We then computed the residuals (absolute values) from each spatial model against the actual AT observed at the held-out station location. We conducted the Wilcoxon test in comparing the daily residuals of two spatial models over yearly periods and across the combined 5 iterations. The Wilcoxon test is also known as a "signed-

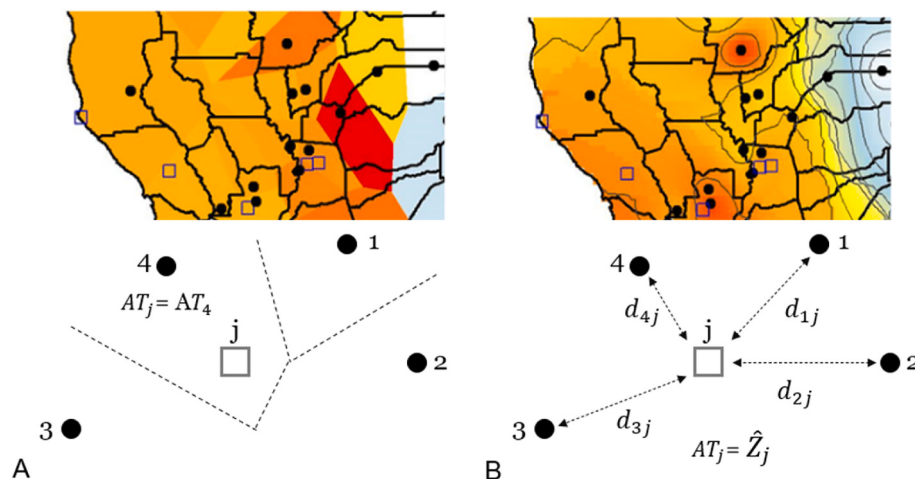


Fig. 4. AT estimated for the held-out test set stations (blank rectangles) using the training set (solid circles) daily records. Plot A (left) shows the uniform spatial surface estimation method. Plot B (right) depicts the spatial interpolation. The regions in shades of blue represent areas with colder AT, while the areas in red represent warmer temperatures.

rank” non-parametric test of paired samples, and used to determine if there is a significant difference between two sets of measurements. The pseudo median is the approximate median distance estimated for the absolute differences between the paired observations (Chaikh et al., 2014). In the case of our validation analysis, the null hypothesis for this test assumed that the median of the paired residuals for the two models is zero, implying no difference in the fit of the two models. On the other hand, the median of the paired residuals is not zero, indicating a difference in the fit between the IDW and NS models.

To quantify the potential improvement, we computed the differences for the mean of daily residuals for the combined iterations, and measured the percentage improvements gained by the spatial interpolation model. In doing so, we subtracted the annual average of the estimated residuals for the IDW interpolation model, from those derived from the NS model. We then divided the differences by the annual average of the NS model residuals.

2.3. Identifying EHEs

We leveraged historical weather data at station level and used the extreme heat definition from Sheridan et al. (2019) to identify EHEs in close proximity to each station. Sheridan et al. define an EHE over a certain period of time, as an episode when the excess heat factor (EHF) exceeds the 85th percentile of all the recorded positive EHF values (Sheridan et al., 2019). EHF is derived as the product of the excess heat (EH) and an acclimatization term (EH_{accl}):

$$EHF = \max(0, EH) * \max(1, EH_{accl}) \quad (2)$$

Where:

$$EH = \max\left(0, \left(\sum_{i=-2}^0 AT_i\right) / 3 - AT_{95th}\right) \quad (3)$$

$$EH_{accl} = \left(\sum_{i=-2}^0 AT_i\right) / 3 - \left(\sum_{i=-32}^{-3} AT_i\right) / 30 \quad (4)$$

Sheridan et al. suggest to account for the acclimatization – the process of adjusting to the changes of weather conditions – one should not only consider the current weather but also assess the conditions that came before for a given location (Sheridan et al., 2019). By evaluating how recent AT is compared to prior period, we can better identify anomalies that can be considered extreme events. Extending on the approach introduced by Sheridan et al., we quantified the

acclimatization term by comparing the average AT of the most recent 3 days to the average AT during the 30-day period preceding those 3 days for a location. In order to determine the EHF baseline distribution (to define the 85th percentile threshold), we computed and sorted the daily values of EHF for the 5-year period from 2017 to 2021 for each station location.

Our algorithm iterated through temporally ordered EHF data and tagged each and every daily record that satisfied EHE criteria. Non-extreme conditions were coded as “0”, and the heat events as “1”. At each station, we “chained” discrete events that were uninterrupted by temporal gaps (i.e., consisted of consecutive days) (Stefanon et al., 2012). Then, for each episode of EHE, we generated a Unique Identifier (UID) by concatenating the events start and end date representing those consecutive days that the event persisted. Finally, reiterating through the compiled records, we calculated the ordinal position of each day within the identified EHE and the “maximum heat” for each station, as the maximum daily temperature observed during an event. By aggregating all the daily records of the events, we introduced and calculated Extreme Heat Magnitude Indicator (EHMI) as the min-max normalized product of the intensity (EHF) and duration of independent events. We then used a spatial interpolation approach to estimate a continuous fine-resolution (600m grids) surface representing EHMI value at daily intervals.

2.3.1. Spatio-temporal delineation of EHE boundaries

Using the spatio-temporal extreme events data, we dynamically estimated the geographic boundary for each event by synthesizing neighboring stations’ status. We implemented a 2-step approach for delineating boundaries of EHEs. First, we used a spatial interpolation approach to estimate a continuous surface representing EHMI value at daily intervals. In this study we employed the Inverse Distance Weighting (IDW) method to estimate the surface. Second, we applied a data-driven threshold and generated closed contours (i.e., regions with the same level of EHMI) to extract geographies impacted by the extreme events. This resulted in a set of estimated zones that captures the spatial extent of dynamic climate events on a daily basis.

2.3.2. IDW interpolation

Spatial Interpolation methods are used to estimate unknown values at a given location based on a set of spatially distributed known observations (Myers, 1994). The IDW interpolation, Thin-Plate Splines (TPS) (Hancock and Hutchinson, 2006) and Kriging methods (Vicente-Serrano et al., 2003) are commonly used methods in climatological studies (Jarvis and Stuart, 2001). We chose the IDW as it could provide a more

computationally efficient solution for our fine-resolution iterative EHE identification algorithm.

The IDW interpolation estimate, \hat{Z}_j is computed as an average value at the point j , using values from nearby locations i , weighted according to the distance. In this formula, d_{ij} denotes the Euclidean distance between the known observations i and the point j . Parameter n represents the weight that applies on the distance, from every i to j . Theoretically, as moving further away from the known point i (in our case weather stations) the influence of the observation decreases relative to the magnitude of parameter n .

$$\hat{Z}_j = \frac{\sum_i Z_i / d_{ij}^n}{\sum_i 1 / d_{ij}^n} \quad (5)$$

2.4. Evaluating the spatio-temporal interpolated surfaces

In order to evaluate our dynamic spatio-temporal EHE delineation method, we mapped the dynamically delineated EHE boundaries over the 9129 census tracts in California at daily intervals. For this study we retrieved the total population of census tracts from the US Census American Community Survey (<https://www.census.gov/programs-surveys/acs/>). Currently, we have extracted from the US Census, the total number of individuals living in that tract (“population size”). The ACS Census data are for 5 year windows and we have the window that reflects 2015–2019.

As the delineated EHE boundaries turned out to be in irregular shapes and orientations, we used a “weighted areal interpolation” approach (Goodchild et al., 1993) and compiled demographic variables for the interpolation method. The weighted areal interpolation is a spatial apportioning method that takes into account the proportion of (partially or fully) overlapping areas between two spatial objects with inconsistent boundaries. It proportionally distributes the variable of interest from one or more objects within the source layer (e.g. actual population at one or multiple zip codes) into one object within the target layer (e.g. estimated population within a certain EHE impacted area). For the NS method, we assumed spatial uniformity and linked each census tract to its nearest station through spatial join operation (Fig. 4, plot A). EHEs are dynamic phenomena, on a certain day one EHE might impact the entire population of the state, the next day it impacts a much smaller proportion of the population, and then ends the next day. We computed the “average impacted population per day of EHE” as a metric to represent the daily impacts of EHEs while extreme heat persists. To calculate this metric, we summed up the daily values of the impacted population throughout the duration of the EHE and divided by the total number of days of the events.

We then calculated the populations and areas impacted across the two approaches and marked the disagreements between the two methodologies under different misclassification types by the nearest-weather station. Through an evaluation in a daily interval, we specified those areas that were identified by the spatio-temporal delineation method but have been missed by the nearest-weather station method as Type 1 misclassification. Accordingly, those census tracts that were only recognized by the nearest-weather station method were categorized as the Type 2 misclassification. This was based on the assumption that the NS approach would be less accurate than the interpolation method implemented in our dynamic spatio-temporal delineation methodology.

2.5. Resources and software

Our informatics pipeline was implemented in the R Statistical Software (v4.2.1) along with the “Tidyverse” packages. We used “sf” library to handle spatial data and t perform geoprocessing operations (Pebesma, 2018). We explored and investigated the quality of collected raw data using “naniar” (Data Structures et al.) and “visdat” (Tierney

and Preliminary Visualisation of Data) packages. Missing values were imputed using “imputeTS” package (Moritz and Bartz-Beielstein, 2017), and the climatological unit conversion was done in “weathermetrics” package (Functions to Convert Between Weather Metrics). The required code for reproducing the pipeline and the paper analyses were organized as modular scripts which is accessible from the project github repository at: <https://github.com/epedram/ehmi>.

We also sought to provide the data sets and our developed data science tools toward FAIR research principles (Findability, Accessibility, Interoperability, and Reuse) (Wilkinson et al., 2016). One prerequisite includes open software and data, not possible if we opted to use proprietary and commercial software and tools.

The computations were performed on a cluster node with 20 cores and 250 GB of memory on the O2 High Performance Compute Cluster, supported by the Research Computing Group, at Harvard Medical School.

3. Results

We compiled a 5-year climatological data set from the State of California and generated a baseline distribution of average daily AT for selected NOAA weather stations (Figs. S2 and S3).

We were able to impute missing values for the short (i.e., 1 to 3 consecutive days) and medium missingness gaps (i.e., from 4 to 18 consecutive days). We ended up with 135 stations with adequate data coverage and aggregated their hourly weather measures into daily values. Based on the derived daily values at stations locations, we estimated two AT spatial surfaces using the IDW interpolation and the NS model.

Table 1 summarizes the results of the Wilcoxon test in comparing the daily residuals of two spatial models over yearly periods. These test results were statistically significant (P-value < 0.05) during all the annual periods between 2017 and 2021, across the combined sampling iterations. Based on these results, we are able to reject the null hypothesis of the Wilcoxon signed-rank test and infer a significant difference in the model performance between the IDW and NS models. In a yearly basis analysis, we observed the IDW model improved upon the NS model, by achieving 15.8%–30.5% smaller mean residual values.

We also calculated R^2 and RMSE to compare the performance of the two spatial methods. When analyzing on a yearly basis, we observed that the IDW model generally outperformed the NS model, achieving R^2 improvement ranging from 2.27% to 7.41% (exception is –3.41% lower performance in 2018). Overall, the interpolation method showed consistent improvement over the study window and produced smaller residuals in estimates of AT.

We identified a wide range of EHE frequencies over a 5-year study period, ranging from 40 distinct events in 2021, to 75 events in 2017. The events’ duration for this period also varied considerably from average of 2.0 days in 2021, to average of 5.1 days in 2020. The longest identified EHE occurred in 2018 with a duration of 11 days. Moreover, the maximum number of distinct EHE days was recorded in 2017 with 51 days of extreme heat, while the minimum of 36 days was observed in 2018 and 2020.

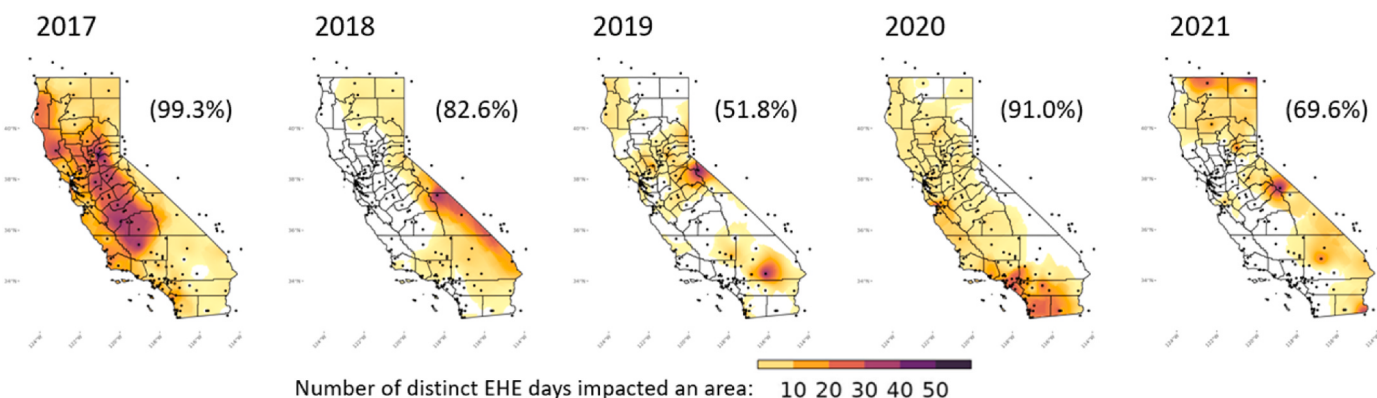
Our spatial interpolation method estimated that a major proportion (more than 50 percent) of California’s land surface was impacted by at least one EHE during the study period (Table 2 and Table S1). However, on a yearly basis, the impacted land areas varied in terms of surface size and location (Fig. 5). While in 2019, only around 52 percent of California’s surface experienced at least one EHE, the maximum impacts were identified in 2017, where almost the entire State was impacted by at least one EHE.

Overall, within the 5-year period of this study, 2017 stands out as the maximum number of EHE (i.e. 75 EHEs) and event days (51 distinct days) were identified in this year. The spatial extent of areas impacted by EHEs at each day is another major factor that has led to the observed widespread impact of the EHEs in 2017. This finding can be explained by

Table 1

Results of the Wilcoxon test for the daily residuals for two spatial models, over the yearly periods.

Year	Method	Wilcoxon Pseudo Median of Absolute Residuals	Wilcoxon Pseudo Median (95% CI)	Mean of Absolute Residuals for estimated AT (95% CI)	Improved by IDW model	RMSE** (Delta in parentheses)	R ² *** (Delta in parentheses)
2017	NS	0.30 ^a	[0.30, 0.34]	4.27 [4.06, 4.49]	28.8%	6.03	0.81
	IDW			3.04 [2.91, 3.17]		4.07 (32.05%)****	0.87 (7.41%)****
2018	NS	0.15 ^a	[0.14, 0.19]	1.84 [1.76, 1.92]	15.8%	4.93	0.88
	IDW			1.55 [1.48, 1.61]		5.03 (2.03%)	0.85 (-3.41%)
2019	NS	-0.19 ^a	[-0.20, -0.19]	2.02 [1.94, 2.11]	21.3%	5.02	0.85
	IDW			1.59 [1.53, 1.66]		4.47 (10.96%)	0.87 (2.35%)
2020	NS	0.04 ^a	[0.00, 0.05]	2.39 [2.3, 2.49]	30.5%	4.83	0.88
	IDW			1.66 [1.6, 1.72]		4.08 (15.53%)	0.90 (2.27%)
2021	NS	0.19 ^a	[0.15, 0.20]	2.19 [2.09, 2.29]	21.5%	5.44	0.83
	IDW			1.72 [1.64, 1.8]		4.70 (13.60%)	0.85 (2.41%)

^a (P-value<0.05) ** in AT (°C). *** Coefficient of Determination. **** percent improvement over NS in parentheses.**Fig. 5.** Number of distinct EHE days impacted an area, along with the spatial distribution and proportion of land areas impacted by at least one EHE (2017–2021). Percent of the land surface impacted by at least one EHE presented in parentheses.**Table 2**

Summary results of the identified EHE over the yearly periods.

	2017	2018	2019	2020	2021
Number of discrete events	75	58	41	71	40
Mean duration of event in days (SE)	3.9 (0.08)	4.8 (0.18)	2.2 (0.1)	5.2 (0.11)	2.0 (0.09)
Longest event in days	9	11	5	10	4
Mean AT (SE) [for the impacted stations and during EHEs]	60.8 (0.39)	58.4 (0.62)	54.2 (1.07)	62.5 (0.39)	55.8 (1.35)
[for all stations year-round]	52.0 (21.9)	30.4 (24.1)	20.8 (20.7)	50.4 (23.0)	29.2 (36.0)
Mean average daily temperature in °C (SE) [for the impacted stations and during EHEs]	26.8 (0.20)	28.1 (0.31)	25.2 (0.57)	26.9 (0.21)	28.4 (0.51)
[for all stations year-round]	16.5 (7.2)	16.2 (7.0)	15.5 (7.1)	16.2 (7.3)	15.9 (7.4)
Maximum AT (hottest) ^a	99	88	103	94	86
Maximum average daily temperature in °C (hottest)	38.6	39.6	41.9	40.6	40.5
Impacted population (average per day of EHE)**	3,337,229	1,729,199	1,129,812	5,488,105	1,063,019
Impacted area (by at least one EHE)	99.3%	82.6%	51.8%	91.0%	69.6%
Mean EHF [for the impacted stations and during EHEs]	151.2	103.4	116.9	122.0	74.4

^a Maximum heat should be interpreted with caution, it may reflect AT observed on one or a few stations and bounded areas. ** The “average impacted population per day of EHE” is a metric to represent the daily impacts of EHEs while extreme heat persists. SE: Standard Error.

the fact that in 2017 California experienced its highest average year-round temperature and average annual temperature (AT) across all the stations.

Fig. 6 plot (A) shows the spatial extent and intensity of EHMI values interpolated for an EHE detected on June 12, 2019. As this figure indicates, the EHMI values change over a smooth spatial gradient corresponding to the heat intensity. Areas in red represent the center of the heat event, and the other colored zones depict the transition areas moderately impacted by the heat event, the white areas indicate unimpacted regions. To delineate the heat events boundaries using the regional EHMI distribution, we applied a statistical threshold corresponding to the 50th percentile of the EHMI value as the cut off criteria to bound or define the events spatially. **Fig. 6** plot (B) illustrates the comparison between the spatial extents of the identified heat events

using both applied methods. In this plot, orange color (“Interpolated surface”) denotes differences between the NS and interpolated approaches. The IDW method tends to create impacted zone boundaries larger than their counterpart zones identified by the NS method.

Fig. 7 illustrates the same comparison over a multi-day dynamic heat event using both applied methods. We performed this comparison on a daily interval and computed the annual levels of misclassified population (**Table 3**).

We found that the spatial interpolation and the NS models have disagreement in estimating impacted populations over time. **Table 3 (A)** illustrates the percentage of the potentially misclassified population to the total impacted population. These statistics were derived from the aggregation of the daily instances of methods disagreement on identifying impacted census tracts using the NS and the IDW approaches.

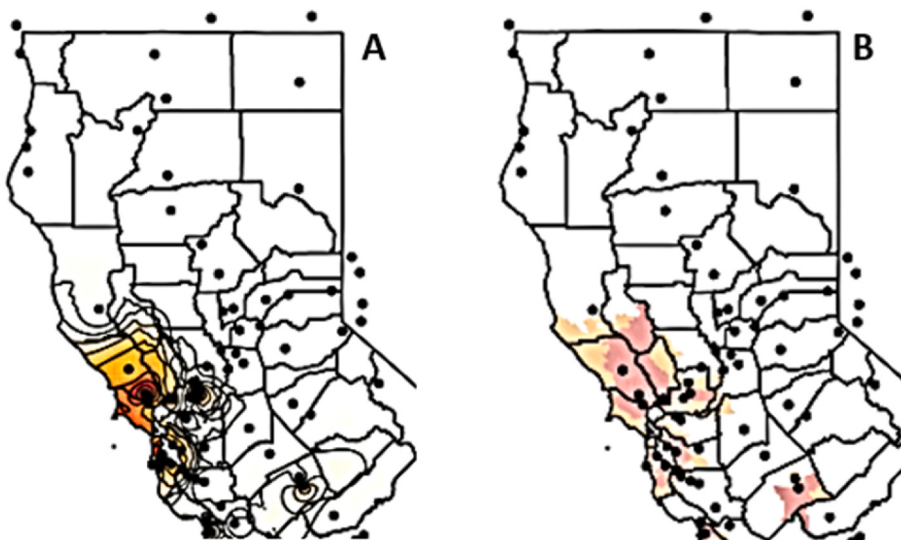


Fig. 6. Plot A (left) Spatial extent of the identified heat events using interpolated surface method. Plot B (right) Comparison of the spatial extents of the identified heat events using both applied methods. Green denotes NS; orange denotes interpolated surface; red denotes both.

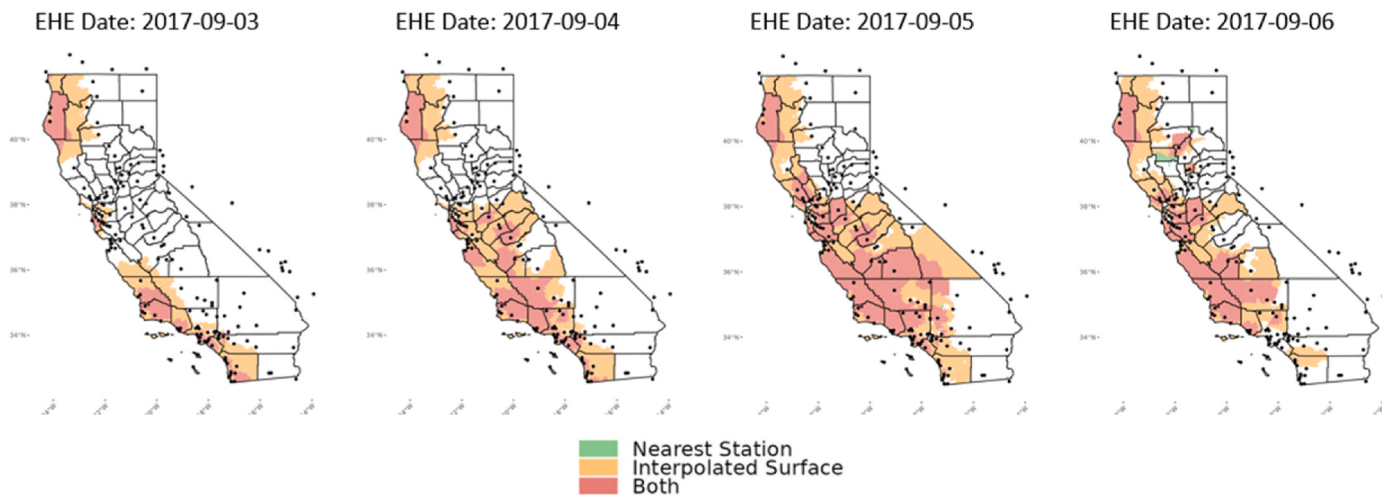


Fig. 7. Comparison of the spatial extents of a multi-day heat event using both methods.

Table 3

(A) Percentage of the potentially misclassified population to the total impacted population by the relative levels of methods disagreement in identifying EHEs.
(B) Proportion of the impacted population by the EHE identification method.

(A) Percentage of the potentially misclassified population to the total impacted population	2017	2018	2019	2020	2021
Methods disagreement at least in:					
40% of EHE days	73.2%	81.5%	83.2%	73.2%	81.9%
60% of EHE days	69.5%	76.0%	79.7%	62.7%	79.8%
80% of EHE days	61.3%	75.7%	75.8%	58.3%	78.0%
(B) Proportion of the impacted population by EHE identification method					
Identified through both methods (method agreement)	11.9%	9.4%	6.3%	19.0%	5.3%
Identified only by IDW interpolation method	87.8%	90.3%	93.3%	80.4%	94.0%
Identified only by NS method	0.3%	0.3%	0.4%	0.6%	0.7%

Fig. 8 shows the spatial distribution of the methods disagreement on impacted census tracts over year 2017. The year by year comparison presented on **Table 3 (A)** shows that by using the standard nearest-

weather station approach, more than 62.7% of the impacted Californians would be misclassified in at least 60% of EHE days. That is they would be (a) mainly identified outside of EHE when under impact, or (b) to a lesser extent, identified under EHE when not.

Table 3 (B) indicates that in general for the period of this analysis, the main methods disagreement can be attributed to type 1 misclassification. It is important to note that the overall levels of methods disagreement consistently remained above the 80.4% level (which was observed in 2020). On average the majority of potentially impacted Californians tend to be overlooked in conventional EHEs impact analysis. In contrast, the type 2 misclassification category is only associated with less than 1% of the total impacted population. For the rest of the impacted population both methods were able to identify the same census tracts under the EHEs impact. For a more detailed example of the differences between the two methods, see [Appendix 1, Fig. S1](#).

4. Discussion

Accurate identification of populations at risk when exposed to EHEs is critical. In the absence of a unified definition for such extreme events ([Kim et al., 2011](#)), researchers often incorporate relative measures of

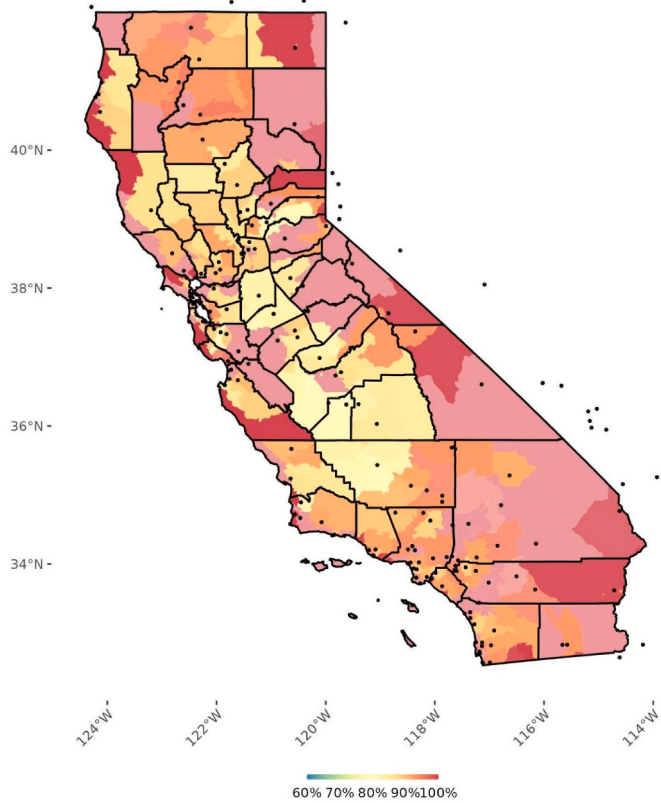


Fig. 8. Spatial distribution of census tracts subject to identification disagreement (Year, 2017). The numbers signify the percentage of extreme heat days that each census tract has been misidentified by either spatial method.

temperature (Steadman, 1984) to identify days in which human thermoregulation is stressed (Epstein and Moran, 2006; Urban and Kyselý, 2014; Ng et al., 2014; Allen and Sheridan, 2018). Aggregate spatial scales such as the county level (Fisher et al., 2017; Isaksen et al., 2016) and metropolitan scale (Sheridan et al., 2019; Anderson and Bell, 2011; Gasparrini et al., 2015; Ishigami et al., 2008; Guo et al., 2017; Michelozzi et al., 2009) have been commonly used in the literature, while fewer studies were conducted at the more disaggregated scales of postal code and neighborhood unit (Elser et al., 2021; Lee et al., 2016; Murage et al., 2020). We also identified a tendency to use grid-based spatial models through leveraging reanalysis and remotely sensed surface temperature data in more recent studies (Nori-Sarma et al., 2022; Tuholske et al., 2021; Sheridan et al., 2020; Spangler et al., 2019; Royé et al., 2020; de Schrijver et al., 2021).

Here, we proposed a spatio-temporal methodology to dynamically delineate the boundaries of EHEs using spatial interpolation of AT at a fine spatial resolution and daily interval. Our developed method provides a more accurate estimate of EHEs and their boundaries compared to the conventional methods such as CDC Heat and Health Tracker (Åström et al., 2011), and California Heat Assessment Tool (Public Health Institute (PHI) et al.). The conventional methods used for surveillance have relied on absolute temperature and or aggregate spatial scales.

Spatio-temporal delineation of extreme heat (and cold) events using the methodology described in this research can enhance precision in definition of exposure depending on the geographic unit of analysis available in epidemiological data. The 600x600-m interpolated grids provide the finest spatial resolution available for extreme heat (and cold) events in the US and therefore can accommodate exposure definition at individual levels or census blocks. However, if an

epidemiological dataset only contains aggregate geographic units (e.g., zip/postal code), spatial allocation methods need to be applied to infer the proportion of the geographic units with population under study.

Our results demonstrate that our method could significantly improve misclassification of populations impacted by EHE. Our method accounts for antecedent climate conditions, as acclimatization is a critical factor to impact the heat events hazards (Anderson and Bell, 2011). The acclimatization term employed in our model enhances signals associated with extraordinary heat conditions relative to both recent days and historical temperature normal for a specific location. Consequently, the implemented model is more adept at detecting dynamic spatial and temporal patterns of EHEs rather than stationary hotspots of regions with hot climate.

We observed a considerable degree of disagreement in areas where weather stations are either widely dispersed or condensed in space. In other words, where few weather stations exist (such as in outer suburban rings and rural areas) or stations are spatially clustered in a very small area (e.g., San Francisco Bay Area), the nearest-weather station method is unable to correctly identify the population and areas under EHE. Since the risk that is raised by an extreme climate event is often amplified by other environmental, socioeconomic and demographic characteristics, this warrants further investigation.

There are limitations to the work presented here. First, the limited spatial extent of this study warrants further more expanded study period covering the entire continental US, considering not only heat, but extreme cold, events. Extreme cold events are of highest priority given their burden on mortality (Gasparrini et al., 2015). Second, to address uncertainties originating from the unit conversions and measurement errors will require cross-validation of climate variables (e.g., temperature) using complementary data sources including remotely sensed data (e.g., land surface temperature). Nevertheless, this study proposes improvements in identifying exposure to extreme heat (and also cold) events via a simple interpolation technique that can easily improve the conventional approach of using the geographically nearest station. Given that both methods (ours and the conventional method) use a derivation of distance to infer the heat index, whether or not the improved accuracy can be attributed to the density of the weather stations can be evaluated in future studies.

We considered the overall exposed population within EHE boundaries to derive the proportion of impacted individuals. While we aimed to approximate this population to assess the impacts of EHEs, we acknowledge that this approach could potentially affect the accuracy of our results.

This study provides spatio-temporal delineations for EHEs in high resolution. To our knowledge, among the publicly accessible temperature data sets, the best spatial resolution is at 1 km provided by Daymet (Thornton et al., 2023), and the land surface temperature dataset by Iowa State University (Zhang et al., 2022). Further, an event boundary often fluctuates on a daily basis. Overlapping this fine-grained data on population data can be challenging due to spatial mismatch in resolution. Perfect spatial overlay can happen when population data is available at the exact coordinates. However, when individual-level or patient-level data is aggregated, spatial appropriation techniques need to be used to overlay the two data sources. For example, when patient data are only available at the postal code level, an approximation via appropriation will introduce noise and may negate some of the improvements that we demonstrate. On the other hand, we claim that the *de facto* standard approaches of assigning the EHE from the closest weather station is simplistic and will bias population-based epidemiological or health services associations and predictions. Such an estimation is sensitive to underneath conditions such as spatial distribution of the weather stations, topography, vegetation and other locational factors. Areas with limited data records also introduce uncertainty to estimates (Hijmans et al., 2005). We aim to test the size of the bias due to aggregation and use of nearest neighbor methods in the future.

We also aim to integrate the spatially identified EHE boundaries,

with individual-level retrospective clinical cohort data which includes information on immediate (e.g., acute hospitalization), disease-specific, and longer-term (e.g. mortality) health outcomes. By linking these datasets with EHEs, we will be able to address specific epidemiological inquiries. One example of involves assessing the relationship between the incidence of extreme heat (or cold) events and the exacerbation of hospitalization within various subgroups of vulnerable individuals, such as the elderly and frail population, and those with specific medical conditions (e.g., cardiovascular disease, heart failure, dementia). Methodologically, our approach involves integrating health-related events based on their spatial and temporal attributes. We will then analyze the event rates before and after the specific extreme events and compare them to a baseline event rate applicable to the at-risk group under study.

We are in the process of cataloging and publicly providing all extreme heat and cold events in the United States for the past 15 years. Future work will incorporate additional variables (e.g., land surface temperature, land cover, elevation) to further improve delineation of extreme heat and cold events.

Authors contributions statement

Pedram Fard: Methodology development, Software, Climatological data curation, Formal analysis, Visualization, Original draft preparation, Ming Kei (Jake) Chung: Software, Computing resources, Hossein Estiri: Funding acquisition, Conceptualization, Validation, Writing – review & editing, Chirag J. Patel: Funding acquisition, Administration, Conceptualization, Writing – review & editing.

Declaration of competing interest

The authors declare that they have no known competing financial interests or personal relationships that could have appeared to influence the work reported in this paper.

Data availability

The link to the code repository can be found within the article.

Acknowledgements

This research has been funded by National Institutes of Health, National Institute on Aging (NIA) through the grant number 1RF1AG074372 and NIEHS R01ES032470. We declare no conflicts of interest. We thank Francesca Dominici for her critical comments on the results and approach.

Appendix A. Supplementary data

Supplementary data to this article can be found online at <https://doi.org/10.1016/j.envres.2023.116984>.

References

- Afrifa-Yamoah, E., Mueller, U.A., Taylor, S.M., Fisher, A.J., 2020. Missing data imputation of high-resolution temporal climate time series data. *Meteorol. Appl.* 27 (1) [Internet]. <https://rmets.onlinelibrary.wiley.com/doi/abs/10.1002/met.1873>.
- Allen, M.J., Sheridan, S.C., 2018. Mortality risks during extreme temperature events (ETEs) using a distributed lag non-linear model. *Int. J. Biometeorol.* 62 (1), 57–67.
- Anderson, G.B., Bell, M.L., 2011. Heat waves in the United States: mortality risk during heat waves and effect modification by heat wave characteristics in 43 U.S. communities. *Environ. Health Perspect.* 119 (2), 210–218.
- Åström, D.O., Forsberg, B., Rocklöv, J., 2011. Heat wave impact on morbidity and mortality in the elderly population: a review of recent studies. *Maturitas* 69 (2), 99–105.
- Wondmagegn, B.Y., Xiang, J., Williams, S., Pisaniello, D., Bi, P., 2019. What do we know about the healthcare costs of extreme heat exposure? A comprehensive literature review. *Sci. Total Environ.* 657, 608–618.
- Cai, J., 2019. Calculate Water Vapor Measures from Temperature and Dew Point [R Package Humidity. version 0.1.5]. Nov 10 [cited 2023 Jul 11]; Available from: <https://cran.r-project.org/web/packages/humidity/index.html>.
- Chaikh, A., Giraud, J.Y., Perrin, E., Bresciani, J.P., Balso, J., 2014. The choice of statistical methods for comparisons of dosimetric data in radiotherapy. *Radiat. Oncol.* 9, 205.
- Cheng, J., Xu, Z., Bambrick, H., Su, H., Tong, S., Hu, W., 2018. Heatwave and elderly mortality: an evaluation of death burden and health costs considering short-term mortality displacement. *Environ. Int.* 115, 334–342.
- Cheng, J., Xu, Z., Bambrick, H., Prescott, V., Wang, N., Zhang, Y., et al., 2019. Cardiorespiratory effects of heatwaves: a systematic review and meta-analysis of global epidemiological evidence. *Environ. Res.* 177, 108610.
- Chowienzyk, K., McCarthy, M.P., Hollis, D., Dyson, E., Lee, M., Coley, D., 2020. Estimating and mapping urban heat islands of the UK by interpolation from the UK Met Office observing network. *Build. Serv. Eng. Res. Technol.* 41 (5), 521–543.
- Chun, Y., Kwan, M.P., Griffith, D.A., 2019. Uncertainty and context in GIScience and geography: challenges in the era of geospatial big data. *Int. J. Geogr. Inf. Sci.* 33 (6), 1131–1134.
- Data Structures, Summaries, and Visualisations for Missing Data [R package nanar. version 0.6.1]. 2021 May 14 [cited 2022 Dec 21]; Available from: <https://cran.r-project.org/web/packages/nanar/index.html>.
- de Schrijver, E., Folly, C.L., Schneider, R., Royé, D., Franco, O.H., Gasparini, A., et al., 2021. A Comparative analysis of the temperature-mortality risks using different weather datasets across heterogeneous regions. *Geohealth* 5 (5), e2020GH000363.
- Delmelle, E.M., Desjardins, M.R., Jung, P., Owusu, C., Lan, Y., Hohl, A., et al., 2022. Uncertainty in geospatial health: challenges and opportunities ahead. *Ann. Epidemiol.* 65, 15–30.
- Ebi, K.L., Capon, A., Berry, P., Broderick, C., de Dear, R., Havenith, G., et al., 2021. Hot weather and heat extremes: health risks. *Lancet* 398 (10301), 698–708.
- Ellis, F.P., Nelson, F., 1978. Mortality in the Elderly in a Heat Wave in New York City, vol. 15. *Environmental Research*, p. 504. [https://doi.org/10.1016/0013-9351\(78\)90129-9](https://doi.org/10.1016/0013-9351(78)90129-9). August 1975 [Internet].
- Elser, H., Parks, R.M., Moghavem, N., Kiang, M.V., Bozinov, N., Henderson, V.W., et al., 2021. Anomalously warm weather and acute care visits in patients with multiple sclerosis: a retrospective study of privately insured individuals in the US. *PLoS Med.* 18 (4), e1003580.
- Epstein, Y., Moran, D.S., 2006. Thermal comfort and the heat stress indices. *Ind. Health* 44 (3), 388–398.
- Fisher, J.A., Jiang, C., Soneja, S.I., Mitchell, C., Puett, R.C., Sapkota, A., 2017. Summertime extreme heat events and increased risk of acute myocardial infarction hospitalizations. *J. Expo. Sci. Environ. Epidemiol.* 27 (3), 276–280.
- Functions to Convert Between Weather Metrics [R package weathermetrics version 1.2.2]. 2016 May 19 [cited 2022 Dec 21]; Available from: <https://cran.r-project.org/web/packages/weathermetrics/index.html>.
- Gasparini, A., Guo, Y., Hashizume, M., Lavigne, E., Zanobetti, A., Schwartz, J., et al., 2015. Mortality risk attributable to high and low ambient temperature: a multicountry observational study. *Lancet* 386 (9991), 369–375.
- Goodchild, M.F., Anselin, L., Deichmann, U., 1993. A Framework for the areal interpolation of socioeconomic data. *Environ. Plan. A* 25 (3), 383–397.
- Gronlund, C.J., Berrocal, V.J., White-Newsome, J.L., Conlon, K.C., O'Neill, M.S., 2015. Vulnerability to extreme heat by socio-demographic characteristics and area green space among the elderly in Michigan, 1990–2007. *Environ. Res.* 136, 449–461.
- Guo, Y., Gasparini, A., Armstrong, B.G., Tawatsupa, B., Tobias, A., Lavigne, E., et al., 2017. Heat Wave and Mortality: A Multicountry. In: Multicommunity Study [Internet], vol. 125. Environmental Health Perspectives, 087006. <https://doi.org/10.1289/ehp1026>.
- Hajat, S., Kosatky, T., 2010. Heat-related mortality: a review and exploration of heterogeneity. *J. Epidemiol. Community Health* 64 (9), 753–760.
- Hancock, P.A., Hutchinson, M.F., 2006. Spatial interpolation of large climate data sets using bivariate thin plate smoothing splines. *Environ. Model. Software* 21 (12), 1684–1694.
- Hass, A.L., Runkle, J.D., Sugg, M.M., 2021. The driving influences of human perception to extreme heat: a scoping review. *Environ. Res.* 197, 111173.
- Hijmans, R.J., Cameron, S.E., Parra, J.L., Jones, P.G., Jarvis, A., 2005. Very high resolution interpolated climate surfaces for global land areas. *Int. J. Climatol.* 25 (15), 1965–1978.
- Hoehne, C.G., Hondula, D.M., Chester, M.V., Eisenman, D.P., Middel, A., Fraser, A.M., et al., 2018. Heat exposure during outdoor activities in the US varies significantly by city, demography, and activity. *Health Place* 54, 1–10.
- Horton, R.M., Mankin, J.S., Lesk, C., Coffel, E., Raymond, C., 2016. A review of recent Advances in research on extreme heat events. *Curr. Clim. Change Rep.* 2 (4), 242–259.
- Ilango, S.D., Weaver, M., Sheridan, P., Schwarz, L., Clemesha, R.E.S., Bruckner, T., et al., 2020. Extreme heat episodes and risk of preterm birth in California, 2005–2013. *Environ. Int.* 137, 105541.
- Isaksen, T.B., Fenske, R.A., Hom, E.K., Ren, Y., Lyons, H., Yost, M.G., 2016. Increased mortality associated with extreme-heat exposure in King County, Washington, 1980–2010. *Int. J. Biometeorol.* 60 (1), 85–98.
- Ishigami, A., Hajat, S., Kovats, R.S., Bisanti, L., Rognoni, M., Russo, A., et al., 2008. An ecological time-series study of heat-related mortality in three European cities. *Environ. Health* 7, 5.
- Jarvis, C.H., Stuart, N., 2001. A comparison among strategies for interpolating maximum and minimum daily air temperatures. Part II: the Interaction between number of guiding variables and the type of interpolation method [Internet]. *J. Appl. Meteorol.* 40 (84), 1075. [https://doi.org/10.1175/1520-0450\(2001\)040.1075](https://doi.org/10.1175/1520-0450(2001)040.1075). Available from.

- Kim, Y.M., Kim, S., Cheong, H.K., Kim, E.H., 2011. Comparison of temperature indexes for the impact assessment of heat stress on heat-related mortality. *Environ Health Toxicol* 26, e2011009.
- Kuehn, L., McCormick, S., 2017. Heat exposure and maternal health in the Face of climate change. *Int J Environ Res Public Health* 14 (8). <https://doi.org/10.3390/ijerph14080853> [Internet].
- Kwan, M.P., 2018. The neighborhood effect averaging Problem (NEAP): an Elusive Confounder of the neighborhood effect. *Int J Environ Res Public Health* [Internet] (9), 15. <https://doi.org/10.3390/ijerph15091841>.
- Lee, M., Shi, L., Zanobetti, A., Schwartz, J.D., 2016. Study on the association between ambient temperature and mortality using spatially resolved exposure data. *Environ. Res.* 151, 610–617.
- Luber, G., McGeehin, M., 2008. Climate change and extreme heat events. *Am. J. Prev. Med.* 35 (5), 429–435.
- Michelozzi, P., Accetta, G., De Sario, M., D'Ippoliti, D., Marino, C., Baccini, M., et al., 2009. High temperature and hospitalizations for cardiovascular and respiratory causes in 12 European cities. *Am. J. Respir. Crit. Care Med.* 179 (5), 383–389.
- Moritz, S., Bartz-Beielstein, T., 2017. ImputeTS: Time series missing value imputation in R *R J* 9 (1), 207.
- Murage, P., Kovats, S., Sarran, C., Taylor, J., McInnes, R., Hajat, S., 2020. What Individual and Neighbourhood-Level Factors Increase the Risk of Heat-Related Mortality? A Case-Crossover Study of over 185,000 Deaths in London using High-Resolution Climate Datasets, vol. 134. *Environment International*, 105292. <https://doi.org/10.1016/j.envint.2019.105292> [Internet].
- Myers, D.E., 1994. Spatial interpolation: an overview. *Geoderma* 62 (1), 17–28.
- Nairn, J.R., Fawcett, R.J.B., 2014. The excess heat factor: a metric for heatwave intensity and its use in classifying heatwave severity. *Int J Environ Res Public Health* 12 (1), 227–253.
- National Climatic Data Center, U.S. Department of Commerce, 2001 [Internet]. Integrated Surface Dataset (Global Hourly). NOAA National Centers for Environmental Information (NCEI) [cited 2022 Dec 19]. Available from: <http://www.ncdc.noaa.gov/access/metadata/landing-page/bin/iso?id=gov.noaa.ncdc:C00532>.
- National Environmental Public Health Tracking Network. Heat & Health Tracker [Internet]. CDC Heat & Health Tracker. Available from: <https://ephtacking.cdc.gov/Applications/heatTracker/>. (Accessed 6 January 2023) <https://www.cdc.gov/nssp/partners/CD-Launches-Heat-and-Health-Tracker.html>.
- Ng, C.F.S., Ueda, K., Ono, M., Nitta, H., Takami, A., 2014. Characterizing the effect of summer temperature on heatstroke-related emergency ambulance dispatches in the Kanto area of Japan. *Int. J. Biometeorol.* 58 (5), 941–948.
- Nori-Sarma, A., Sun, S., Sun, Y., Spangler, K.R., Oblath, R., Galea, S., et al., 2022. Association between ambient heat and risk of emergency Department visits for mental health among US Adults, 2010 to 2019. *JAMA Psychiatr.* 79 (4), 341–349. <https://doi.org/10.1001/jamapsychiatry.2021> [Internet]. 4369.
- Pebesma, E., 2018. Others. Simple Features for R: Standardized Support for spatial Vector data. *The R Journal* 10 (1), 439–446. <https://doi.org/10.32614/RJ-2018-009>. URL.
- Peckham, S.E., 2017. The Weather Research and Forecasting Model: Overview, System Efforts, and Future Directions. *American Meteorological Society*, p. 21.
- Public Health Institute (PHI), Four Twenty Seven, Argos Analytics, Habitat Seven. California Heat Assessment Tool [Internet]. California Heat Assessment Tool. [cited 2023 Jan 6]. Available from: <https://www.cal-heat.org/>.
- Romanello, M., Di Napoli, C., Drummond, P., Green, C., Kennard, H., Lampard, P., et al., 2022. The 2022 report of the Lancet Countdown on health and climate change: health at the mercy of fossil fuels. *Lancet* 400 (10363), 1619–1654.
- Royé, D., Íñiguez, C., Tobías, A., 2020. Comparison of temperature–mortality associations using observed weather station and reanalysis data in 52 Spanish cities. *Environ. Res.* 183, 109237.
- Schuman, S.H., 1972. Patterns of urban heat-wave deaths and implications for prevention: data from New York and St. Louis during July, 1966. *Environ. Res.* 5 (1), 59–75.
- Sheridan, S.C., Lee, C.C., 2018. Temporal trends in absolute and relative extreme temperature events across north America. *J. Geophys. Res.* 123 (21), 11–898.
- Sheridan, S.C., Lee, C.C., Allen, M.J., 2019. The mortality Response to absolute and relative temperature extremes. *Int J Environ Res Public Health* (9), 16. <https://doi.org/10.3390/ijerph16091493> [Internet].
- Sheridan, S.C., Lee, C.C., Smith, E.T., 2020. A comparison between station observations and reanalysis data in the identification of extreme temperature events. *Geophys Res Lett* [Internet] 47 (15). Available from: <https://onlinelibrary.wiley.com/doi/10.1029/2020GL088120>.
- Sherwood, S.C., Huber, M., 2010. An adaptability limit to climate change due to heat stress. *Proc Natl Acad Sci U S A* 107 (21), 9552–9555.
- Soneja, S., Jiang, C., Fisher, J., Upperman, C.R., Mitchell, C., Sapkota, A., 2016. Exposure to extreme heat and precipitation events associated with increased risk of hospitalization for asthma in Maryland. *U.S.A. Environ Health.* 15 (1), 57.
- Spangler, K.R., Weinberger, K.R., Wellenius, G.A., 2019. Suitability of gridded climate datasets for use in environmental epidemiology. *J. Expo. Sci. Environ. Epidemiol.* 29 (6), 777–789.
- Steadman, R.G., 1984. A Universal scale of apparent temperature. *J. Appl. Meteorol. Climatol.* 23 (12), 1674–1687.
- Stefanon, M., D'Andrea, F., Drobinski, P., 2012. Heatwave classification over Europe and the Mediterranean region. *Environ. Res. Lett.* 7 (1), 014023.
- Thompson, R., Hornigold, R., Page, L., Waite, T., 2018. Associations between high ambient temperatures and heat waves with mental health outcomes: a systematic review. *Publ. Health* 161, 171–191.
- Thornton, M.M., Shrestha, R., Wei, Y., Thornton, P.E., Kao, S., 2023. version 4 R1 [Internet]. [cited Daymet: Daily surface weather data on a 1-km grid for north America. Jan 3]. Available from: https://daac.ornl.gov/DAYMET/guides/Daymet_Daily_V4R1.html.
- Tierney, N., Preliminary Visualisation of Data [R package visdat version 0.5.3]. 2019 Feb 15 [cited 2022 Dec 21]; Available from: <https://cloud.r-project.org/web/package/s/visdat/index.html>.
- Tuholske, C., Taylor, K., Funk, C., Verdin, A., Sweeney, S., Grace, K., et al., 2021. Global urban population exposure to extreme heat. *Proc Natl Acad Sci U S A* [Internet] 118 (41). <https://doi.org/10.1073/pnas.2024792118>.
- Urban, A., Kysely, J., 2014. Comparison of UTCI with other thermal indices in the assessment of heat and cold effects on cardiovascular mortality in the Czech Republic. *Int J Environ Res Public Health* 11 (1), 952–967.
- Vaneckova, P., Beggs, P.J., Jacobson, C.R., 2010. Spatial analysis of heat-related mortality among the elderly between 1993 and 2004 in Sydney, Australia. *Soc. Sci. Med.* 70 (2), 293–304.
- Vanossi, J.K., Herdt, A.J., Lochbaum, M.R., 2017. Effects of physical activity and shade on the heat balance and thermal perceptions of children in a playground microclimate. *Build. Environ.* 126, 119–131.
- Vicente-Serrano, S.M., Saz-Sánchez, M.A., Cuadrat, J.M., 2003. Comparative analysis of interpolation methods in the middle Ebro Valley (Spain): application to annual precipitation and temperature. *Clim. Res.* 24, 161–180.
- Wilkinson, M.D., Dumontier, M., Ijj, Aalbersberg, Appleton, G., Axton, M., Baak, A., et al., 2016. The FAIR Guiding Principles for scientific data management and stewardship. *Sci. Data* 3, 160018.
- Zhang, Y., Nitschke, M., Krackowizer, A., Dear, K., Pisaniello, D., Weinstein, P., et al., 2017. Risk factors for deaths during the 2009 heat wave in Adelaide, Australia: a matched case-control study. *Int. J. Biometeorol.* 61 (1), 35–47.
- Zhang, T., Zhou, Y., Zhu, Z., Li, X., Asrar, G.R., 2022. A global seamless 1 km resolution daily land surface temperature dataset (2003–2020). *Earth Syst. Sci. Data* 14 (2), 651–664.